INTERNATIONAL JOURNAL FOR RESEARCH

IN APPLIED SCIENCE & ENGINEERING TECHNOLOGY

Experimental Investigation of Fatigue Properties of Udimet (Su-720) at Different Temperatures

Kanchanapally Akhila[1], Dr. J. Suresh Kumar[2]

[1, 2] *Department of Mechanical Engineering, JNTUH College of Engineering, Kukatpally, Hyderabad, India*

Abstract: Fatigue is one of the most predominating factors for causing failure in metals constituting around 90% of failures occurring in strong elements. Experimentation has proved that Nickel alloys have good Fatigue properties. The temperatures at the turbine end of the engines ranges from as high as 700^oC to 1000^oC. The materials used for the turbine disc should sustain high temperatures, corrosive and oxidizing environments. Ni-based superalloys such as Su-720 alloy have been used in gas turbines as discs at high temperature because of its excellent high temperature mechanical properties. The objective of the present work is to study the low cycle fatigue ($< 10^5$ cycles) behaviour of Nickel-based Super alloy, Su-720 specimen which is used in aircrafts engines compressor disc at temperatures up to 750^oC under strain control tests. The inter relationships between microstructure factors and properties of the specimen are analysed using Optical microscope. Material extracted from a forged and annealed (at 730^oC) Su-720 disc is studied. To study the fatigue properties of the material, testing is done at different locations of the disc under different loading and straining conditions.
Keywords: Nickel , Superalloys , Turbine blades , Low cycle fatigue, Fatigue failure , Microstructure-based models.

I. INTRODUCTION

Aero-engine is the core of aircraft which generates the required mechanical power. When gas passes through the jet engine, then the heat generated from the burning of fuel transforms into the kinetic energy with the increment of gas inside the engine. The gas squirts out at high speed and provides the thrust to the plane. During the operation of this cycle different temperatures are obtained. The high temperatures involved during this process will not resist by using single alloy or only one type of materials and it is uncontrollable when the temperatures exceed very high and sometimes may reach almost close to melting point. Most of the materials could not sustain at high temperatures which leads to the failure of the engine parts. To overcome those limitations and retaining the material properties at high temperatures, to resist against the failures of mechanical properties such as creep, fatigue and corrosion at high temperatures and whenever there is a significant resistance to loading under static, fatigue and creep conditions is required, then SUPER ALLOYS are emerged as the materials of choice against all the limitations at higher temperatures.

A super alloy is an alloy that exhibits several key characteristics such as excellent mechanical strength, resistance to thermal creep deformation, good surface stability, and resistance to corrosion or oxidation. Generally, there are 3 types of super alloys-Ti based, Ni based and Fe based. Ni based super alloy is considered in this project which is the most widely used super alloy at high temperatures. Nickel is the fifth most abundant element on earth. The atomic number is 28, and this places it in the first row of the d block of transition metals alongside iron and cobalt. The atomic weight is 58.71, the weighted average of the five stable isotopes are 58, 60, 61, 62 and 64, which are found with probabilities 67.7%, 26.2%, 1.25%, 3.66% and 1.16%, respectively. The crystal structure is face-centred cubic (FCC), from ambient conditions to the melting point, 1455□ which represents an absolute limit for the temperature capability of the nickel-based super alloys. The density under ambient conditions is 8907 kg/m³. Thus, compared with other metals used for aerospace applications, for example, Ti (4508 kg/m³) and Al (2698 kg/m³), Ni is rather dense. This is a consequence of a small inter atomic distance, arising from the strong cohesion provided by the outer d electrons – a characteristic of the transition metals.

II. NICKEL-BASED SUPER ALLOYS (SU-720 UDIMET)

Nickel-Based super alloys are an unusual class of metallic materials with an exceptional combination of high temperature strength, toughness, and resistance to degradation in corrosive or oxidizing environments. These materials are widely used in aircraft and power-generation turbines, rocket engines, and other challenging environments, including nuclear power and chemical processing plants. Nickel-based super alloys typically constitute 40–50% of the total weight of an aircraft engine and are used most extensively in the combustor and turbine sections of the engine where elevated temperatures are maintained during operation. Creep-resistant

turbine blades and vanes are typically fabricated by complex investment casting procedures that are essential for introduction of elaborate cooling schemes and for control of grain structure. Such components may contain equiaxed grains or columnar grains, or may be cast as single crystals, completely eliminating all high-angle grain boundaries. When significant resistance to loading under static, fatigue and creep conditions is required, the nickel-base super alloys have emerged as the materials of choice for high temperature applications. This is particularly true when operating temperatures are beyond about 800°C.

Udimet 720 is a cast-wrought nickel base super alloy which was originally used for land-based gas turbine blades. Work is being done to develop this alloy for high strength disks applications. Super alloys have been developed for specific, specialized properties and applications. One of the main applications for nickel-based super alloys is gas-turbine-engine disc components for land-based power generation and aircraft propulsion. Turbine engines create harsh environments for materials due to the high operating temperatures and stress levels. Hot tensile tests were performed to define temperature and strain rate parameters for conventional, hot die and super plastic forging. This information was used to select forging parameters for disk type pancakes. Heat treatments were developed to produce mechanical properties suitable for disks. U720 is a high strength corrosion resistant nickel base super alloy precipitation strengthened by γ; $Ni_3Ti(Al)$ and solid solution strengthened by Mo, W, Cr, and Co. When solution treated at 1168°C, stabilized and double aged, U720 has strength and stress rupture properties comparable to IN738 at temperatures from 593 to 871°C. However, U720 is unique in that it has superior stress corrosion resistance in low temperature (704°C) sulphate/chloride environments. Whitlow et al. have shown thatU720 retains a much higher percentage of its rupture life when exposed to a mixture of Na_2SO4, $MgSO_4$ and NaCl than Udimet 710, U500, IN738, IN939 and other Ni-base blading alloys. The explanation for this is found in the alloy chemistry and microstructure. U720 contains 0.035C and 0.033B.A parallel benefit of the U720 chemistry and grain boundary structure is enhanced impact resistance in long term service.

U720 impact resistance actually increases after a 10,000-hourexposure at 871°C compared to the severe degradation of impact resistance of U710. Cooper et al. have suggested that the precipitation of $Cr_{23}(C, B)_6$ during heat treatment impedes the formation of $Cr_{23}C_6$ in service environments and thereby improves impact resistance. The impact resistance of other high strength super alloys is reported to decrease similarly to that of U710.This work on the development of U720 for high strength disk applications was based on the realization that reducing the solution temperature in combination with a modified aging treatment raises U720 yield strength substantially in the range of 650°C to 760°C.

Table 2.1 Composition of UDIMET

Alloy	Cr	Ni	Co	Mo	W	Nb	Ti	Al	Fe	C	B	Other
Udimet 720	18	55	14.8	3	1.25	—	5	2.5	—	0.035	0.033	0.03 Zr

The high contents of chromium and molybdenum could provide resistance to corrosive media and high-temperature environments. . Besides, the minor contents of aluminum and titanium could lead to the formation of γ′ phase, which was helpful to improve the creep strength of nickel-based alloys. The addition of cobalt and titanium to Udimet 720 increases the temperature and flow stress capability. It is known that cobalt modifies the solubility of the gamma prime phase in the gamma phase, raises the Solidus temperature, lowers the gamma prime solvus temperature and lowers the stacking fault energy. The addition of titanium increases the Volume fraction of gamma prime phase by forming Co Ti with the same crystal structure as NiAl.

A metal subjected to a repetitive or fluctuating stress will fail at a stress much lower than that required to cause fracture on a single application of load. Fatigue has become progressively more prevalent as technology has developed a greater amount of equipment, such as automobiles, aircraft compressors, pumps, turbines, etc., subject to repeated loading and vibration, until today it is often stated that fatigue accounts for at least 90 percent of all service failures due to mechanical causes.
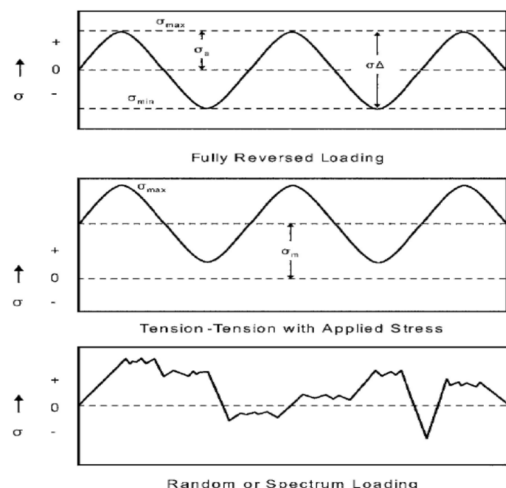
Figure 2.1: Various types of fatigue loadings applied

A fluctuating stress is made up of two components: mean or steady stress, σ_m and alternating or variable stress, σ_a. The stress range, σ_r, is the difference between the maximum and minimum stress in a cycle:

Cyclic stress range: $\Delta\sigma = \sigma_{max} - \sigma_{min}$…………………………(2.1)

The alternating stress or cyclic stress amplitude is one-half the stress range:

Cyclicstressrange: $\Delta\sigma = \sigma_{max} - \sigma_{min}$…………………(2.2)

The mean stress is the algebraic average of the maximum and minimum stress in the cycle

Mean stress: $\sigma_m = \frac{\sigma_{max}+\sigma_{min}}{2}$…………………(2.3)

Two ratios frequently used in presenting fatigue data are:

Stress ratio: $R = \frac{\sigma_{min}}{\sigma_{max}}$…………………(2.4)

Amplitude ratio: $A = \frac{\sigma_a}{\sigma_m} = \frac{1-R}{1+R}$…………………(2.5)

In Low cycle fatigue, during cyclic loading within the elastic regime, stress and strain are directly related through the elastic modulus. However, for cyclic loading that produces plastic strains, the responses are more complex and form a hysteresis loop Fig 2.2. From point O up to point A, the component is in tension. On unloading, the strain response of the specimen follows the curve from A to D. At D, the component is under no stress. As the component is subjected to compressive stress, the strain response follows the curve from D to B. Releasing the compressive stress from B and re applying tensile stress, the component stress-strain condition returns to point A along the curve defined by B, C, and A. Points A and B represent the cyclic stress and strain limits. The total strain, De, consists of both elastic and plastic components. The hysteresis loops reflect continuous changes of stress and strain in the fatigue test. The shape of the hysteresis loop will change during the process of fatigue tests.
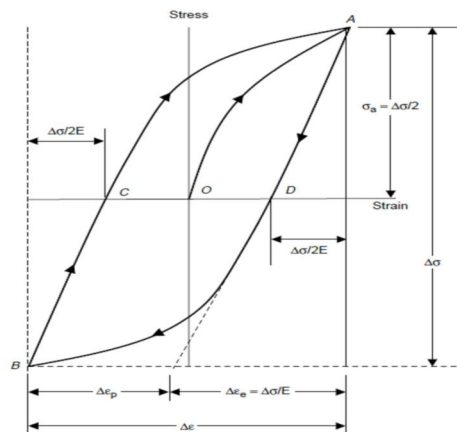

Figure 2.2. Cyclic stress – strain hysteresis loop

For fatigue tests, after the initial maximum loading, the stress-strain response develops into a mechanical hysteresis loop when subjected to one loading cycle. The stress-strain relation tends to be stable gradually and then forms a stable hysteresis loop. The hysteresis loops are given by those at the first cycle (N = 1) and at the mid-life (N = N_f/2, where N_f is the number of cycles to failure). It can be observed from fig.2.2 that the hysteresis loops shift downwards slightly with the increase of the number of cycles in the LCF tests. The downward shift of hysteresis loop is a characteristic of the LCF tests for the super alloy.

$$\Delta\varepsilon = \Delta\varepsilon_e + \Delta\varepsilon_p \ldots\ldots\ldots\ldots\ldots (2.6)$$

Where $\Delta\varepsilon e$ is the elastic strain and $\Delta\varepsilon_e = \Delta\sigma/E$, and $\Delta\varepsilon_p$ is the plastic strain and $\Delta\varepsilon_p$ is the width of the loop at its centre, that is, the distance CD in Fig2.2. The area of the hysteresis loop is equal to the work done or the energy loss per cycle. In cyclic strain-controlled fatigue, the strain amplitude is held constant during cycling. Since plastic deformation is not completely reversible, the stress-strain response during cycling can change, largely depending on the initial condition of the metal. The metal can either undergo cyclic strain hardening, cyclic strain softening, or remain stable. Cyclic strain hardening and softening are illustrated schematically in Fig. 2.3. In both cases, the hysteresis loops change with successive cycles. Cyclic hardening leads to increasing peak strain with increasing cycles, while cyclic softening results in decreasing strain levels with increasing cycles. In general, strong metals tend to cyclically soften, and low-strength metals tend to cyclically harden. However, the hysteresis loop tends to stabilize after a few hundred cycles, when the material attains a stable condition for the imposed strain level. Typically, metals harden if $\sigma_u/\sigma_y \geq 1:4$ and soften if $\sigma_u/\sigma_y \leq 1:2$. The reason for hardening or softening is related to the dislocation microstructure of the metal. When the metal is highly work hardened and the dislocation density is high, cyclic strain allows the rearrangement of dislocations into more stable networks, thereby reducing the stress at which plastic deformation occurs. Conversely, when the initial dislocation density is low, the cyclic strain increases the dislocation density, increasing the amount of elastic strain and stress on the material.

Low-cycle fatigue test data are often presented as a plot of the plastic strain range $\Delta\varepsilon_p$, versus cycles to failure, N. When plotted on log-log coordinates, a straight line is obtained that is described by the Coffin-Manson relation:

$$\frac{\Delta\varepsilon_p}{2} = \varepsilon'_f * (2N)^c \ldots\ldots\ldots\ldots\ldots (2.7)$$

Where $\Delta\varepsilon_p/2$ is the plastic strain amplitude, and ε'_f is the fatigue ductility coefficient defined by the strain intercept at 2N=1. For many metals, ε'_f is approximately equal to the true fracture strain, ε_f. 2N is the number of strain reversals to failure, where one cycle is two reversals, and c is the fatigue ductility exponent, which usually varies between -0.5 and -0.7. A smaller value of c results in longer fatigue lives.

The Basquin's equation, which describes the high-cycle, low-strain regime where the nominal strains are elastic, is:

$$\sigma_a = \frac{\Delta\varepsilon_e}{2} * E = \frac{\sigma'_f}{E} * (2N)^b \ldots\ldots\ldots\ldots\ldots (2.8)$$

Where σ_a is the alternating stress amplitude, $\Delta\varepsilon_e/2$ is the elastic strain amplitude, E is the modulus of elasticity, and σ'_f is the fatigue strength coefficient, defined as the stress intercept at 2N=1. σ'_f is approximately equal to the true fracture stress, σ_f. 2N is the number of load reversals to failure, and b is the fatigue strength exponent, which varies for most metals between -0.05 and -0.12. A smaller b results in a longer fatigue life.
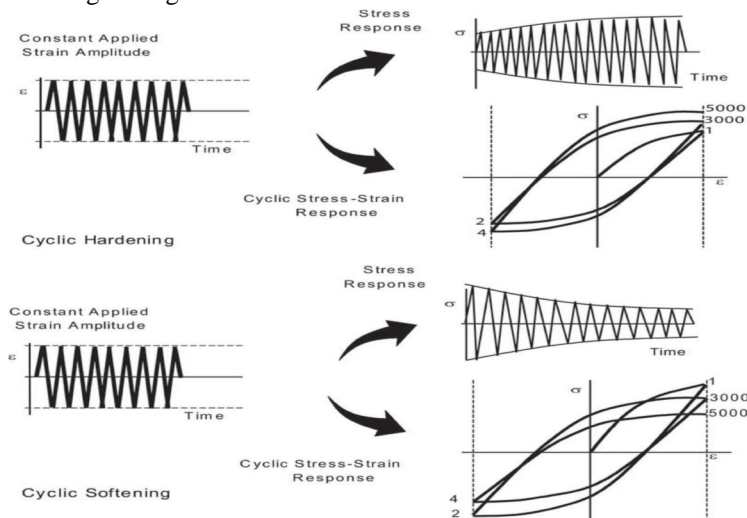

Figure 2.3. Cyclic hardening and cyclic softening

Combining Basquin's equation and the Coffin-Manson equation gives an equation that can be used to estimate the entire range of fatigue lives:

$$\frac{\Delta\varepsilon}{2} = \frac{\Delta\varepsilon_e}{2} + \frac{\Delta\varepsilon_p}{2} \dots\dots\dots\dots\dots (2.9)$$

$$\frac{\Delta\varepsilon}{2} = \frac{\sigma'_f}{E} * (2N)^b + \varepsilon'_f * (2N)^c \dots\dots\dots\dots (2.10)$$

The fatigue strain-life curve tends toward the plastic curve at large strain amplitudes and toward the elastic curve at small strain amplitudes (Fig. 2.4). For high-cycle strain conditions, ductile metals have the longest lives while at low-cycle strain conditions, strong metals have the longest lives.
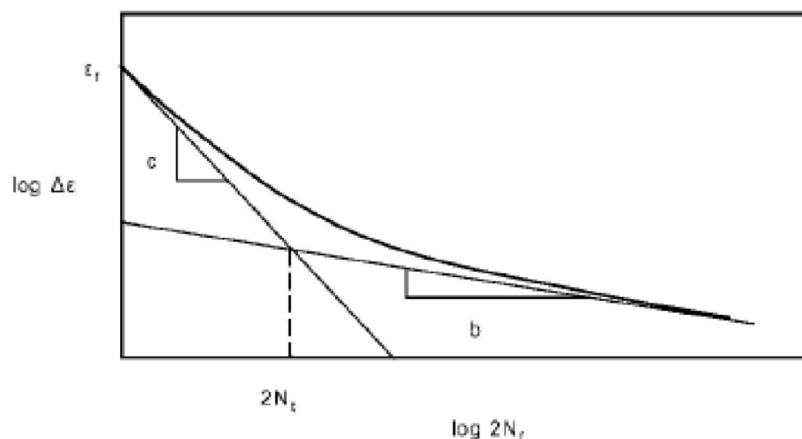
Figure 2.4. Fatigue life in terms of total strain

III. EXPERIMENTAL PROCEDURE AND METHODOLOGY

A. Low Cycle Fatigue Machine and Testing

1) *Strain controlled fatigue:* Strain controlled fatigue is a phenomenon that is influenced by the same variables that influence load-controlled fatigue. In particular, total cyclic strain should be measured and cyclic plastic strain should be determined. Furthermore, either of these strains typically is used to establish cyclic limits; total strain is usually controlled throughout the cycle. The uniqueness if this practice and the results that it yields are the determination of the cyclic stresses and strains at any time during the test. Likewise, the presence of non-zero mean strains and varying environmental conditions may alter fatigue life as compared with the constant amplitude, fully reversed tests. Care must be exercised in analyzing and interpreting the data in such cases. Strain-controlled fatigue can be an important consideration in the design of industrial products. It is important in the situation where components undergo either mechanically or thermally induced cyclic plastic strains that cause failure within relatively few (That is, approximately $< 10^5$) cycles. Strain controlled fatigue test results are useful in the areas of mechanical design as well as materials research and development, process and quality control, product performance, and failure analysis. Results of a strain-controlled fatigue test program may be used in the formulation of empirical relationships between the cyclic variables of stress, total strain, plastic strain and fatigue life. The effect of these strains on the fatigue life can be studied.

2) *Testing Standards*

a) *Testing Machine:* Testing should be conducted with a tension compression fatigue testing machine that has been verified in accordance with their respective standard practices. Testing machine should permit cycling between constant strain limits.

b) *Strain Control:* Testing machine controls should permit cycling between constant strain limits. If material behaviour permits (for example, aging effects do not hinder), control stability should be such that the strain maximum and minimum is repeatable over the test duration to within 1% of the range between maximum and minimum control limits.

c) *Extensometers:* Extensometers should be employed for the purpose of measuring deformation in gauge section. They should be suitable for dynamic measurements over long periods of time. The non-self-contained extensometers may be of two major types: contacting and non-contacting type extensometers. The output of extensometer or auxiliary device of extensometer system should be suitable for control purposes, readout and recording.

d) *Data Recording Strips:* Analogue strip chart and X-Y recorders or their digital equivalent should be considered a minimum requirement for data collection.

e) *Note 1:* Accuracy of the recording strips should be kept within 1% of full scale. Analogue/digital devices are available that include maximum and minimum limit detection, maximum-minimum memory, and under peak detection.

f) *Note 2:* Data acquisition characteristics such as sampling frequency and data skew between force and deformation (stress and strain) channels can affect hysteresis loop presentation on an X-Y recorder used in digital recording systems. It is recommended that these characteristics be taken into consideration along with the strain rate or frequency of the cycling to determine that the hysteresis plots are within the required error limits. In digital type recording devices sufficient number of simultaneous data pairs has to be taken for both the ascending segment and descending segment of the hysteresis loop to adequately determine the range of loop.

g) *Cycle Counter:* A cycle counter shall be used to indicate total accumulated cycles of loading or straining. An elapsed time indicator is a desirable adjunct to the cycle counter to provide an excellent check of both frequency and the current cycle counter.

h) *Calibration:* The calibration interval of all electronic and transducer systems should be performed in accordance with the manufacturer's recommendations; in the absence of these, the interval should be no greater that six months and even more frequent if necessary to maintain required accuracy. Calibration should be checked whenever accuracy is a doubt.

3) *Material And Specimen Selection:* Triple-melted, close-die forging of Su-720 was used for the present investigation. The nominal composition of the alloy is (Cr: 18, Ni:55, Co:14.8, Mo:3,W:1.25, Ti:5, Al:2.5, C:0.035, B:0.033,0.03Zr) as obtained from the supplier. Ingot for forging was obtained by triple-melted vacuum consumable re-melt procedure (VAR).The forging was solution treated at 960°C for 1h, water quenched and annealed at 700 °C for 2h and then air-cooled (AC). The forging was carried out below β transus temperature to meet the forging specification of GTRE, DRDO. This experimental procedure involves extraction of samples from three regions of the already manufactured stage 3 compressor disc with Su-720 alloy. The layout of rim, web and bore regions of the disc is shown in the below figure 3.2.
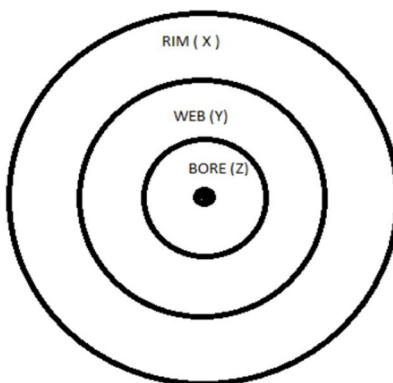

Figure 3.1: Sections of compressor disc

The compressor disc is divided into three regions consisting of the central bore(Z), middle web(Y) and outer rim(X) region. Samples have been taken from the three regions in the tangential and radial directions. The effect of tangential loading on the rotating disc is more on the rim region as it is the outer portion of the disc. The radial loading is more in the bore region as it is nearer to the central shaft. Hence more samples have been taken from rim in tangential direction and bore in radial direction.

Nomenclature of Specimen I.D.:

XTL=Specimen taken from Rim region in tangential loading direction.

XRL= Specimen taken from Rim region in radial loading direction.

YTL= Specimen taken from Web region in tangential loading direction.

YRL= Specimen taken from Web region in radial loading direction.

ZTL= Specimen taken from Bore region in tangential loading direction.

ZRL= Specimen taken from Bore region in radial loading direction.

The dimensions of the specimen taken for testing on LCF testing machine are as listed below

Table 3.1: The dimensions of the Su-720 LCF standard specimen as per ASTM

Gauge Diameter (mm)	Gauge Length (mm)	Shoulder Length (mm)	Total Length (mm)	Thread length (mm)	Radius (mm)	Surface Finish (Ra)
4.5 ± 0.05	12 ± 0.1	36 ± 0.1	62 ± 1.0	13 ± 0.5	17 ± 0.05	0.2
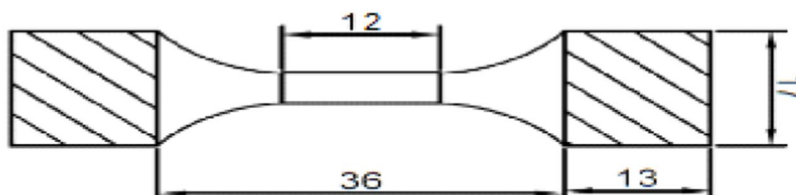
Figure 3.2: Su-720 LCF standard Specimen

16 samples have been tested at 4 different temperatures overall. At RT (Ambient room temperature), 650℃, 700℃ and 750℃, 4 samples each are tested with 4 different strain ranges (0.0002, 0.00035, 0.0005 and 0.00065) have been tested. The minimum and maximum strains applied is listed in the below table 3.2.

Table 3.2: Minimum and maximum strains applied for testing Su-720 alloy

S.No.	Min strain (mm/mm)	Max strain (mm/mm)	Strain range
1	0.0002	0.004	0.0038
2	0.00035	0.007	0.00665
3	0.0005	0.01	0.0095
4	0.00065	0.013	0.01235

Complete testing has been done maintaining a constant strain cycling frequency of 0.3Hz. The specimens taken with their loading, temperature of testing, remarks in data obtained are tabulated in the table 3.3.

Table 3.3: Specimens tested at room temperature and elevated temperatures 650□, 700□, 750□.

Tempurature Strain range		25□	650□	700□	750□
0.0038	Specimen ID	XTL-9	XTL-5	XTL-1	XTL-13
	No.of cycles	100001	10001	100001	100001
0.00665	Specimen ID	XTL-10	XTL-6	XTL-2	XTL-14
	No.of cycles	63389	48042	100001	34783
0.0095	Specimen ID	XTL-11	XTL-7	XTL-3	XTL-15
	No.of cycles	15077	6853	2867	3782
0.01235	Specimen ID	XTL-12	XTL-8	XTL-4	XTL-16
	No.of cycles	6915	1474	720	542

4) *Optical Microscopic Testing On Parent Material:* Microscopy has been performed on the parent metal at the rim, web and bore regions of the Su-720 disc at 100x and 500x magnification. The sample is etched with Keller's reagent.

5) *Scanning Electron Microscopic Inspection:* Striations are micro structural details that are best examined with a scanning electron microscope and are not visible to the naked eye. Frequently, visible examination of a fatigued surface will reveal a series of concentric markings on the surface, referred to as beach marks. These are present as a result of stress changes during fatigue, for example, the starting and stopping of a rotating shaft. Each of the beach marks can contain thousands or even tens of thousands of fatigue cycles. The results obtained from scanning electron microscopy are shown in the later section. 8 out of 16 specimens tested at 25℃, 650℃, 700℃, 750℃ each taken from one location i.e., XTL are selected for the observation of microstructures. To observe the microstructure of any specimen, first it is belt grinded, then polished with silicon carbide papers of different grades (100,400,800 and 1000). The etching agent Keller's is used to etch the grain boundaries of these specimens. Then microstructures of these specimens are observed on electron microscope of 100X and 500X magnification. The microstructures are as follows.
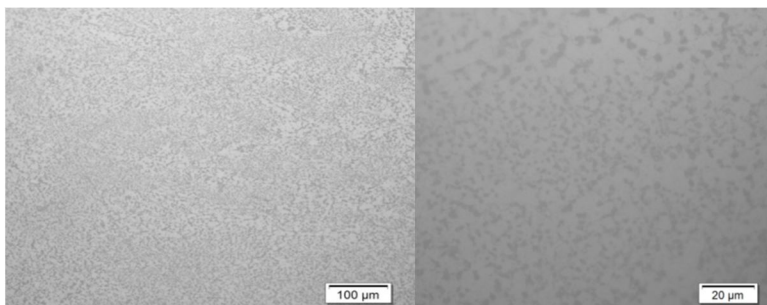

Figure 3.3. Microstructure at rim region in tangential direction at 700☐ (XTL-3) with 100x & 500x magnification at the strain range 0.0095
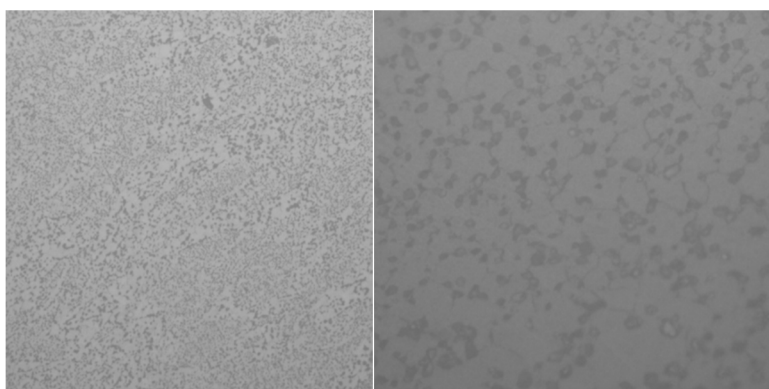

Figure 3.4. Microstructure at rim region in tangential direction at 700☐ (XTL-4) with 100x & 500x magnification at the strain range 0.01235
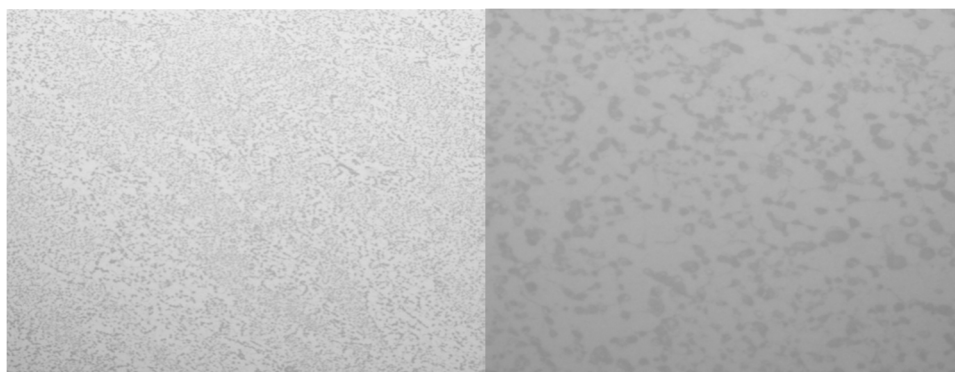

Figure 3.5. Microstructure at rim region in tangential direction at 650☐ (XTL-6) with 100x & 500x magnification at the strain range 0.00665
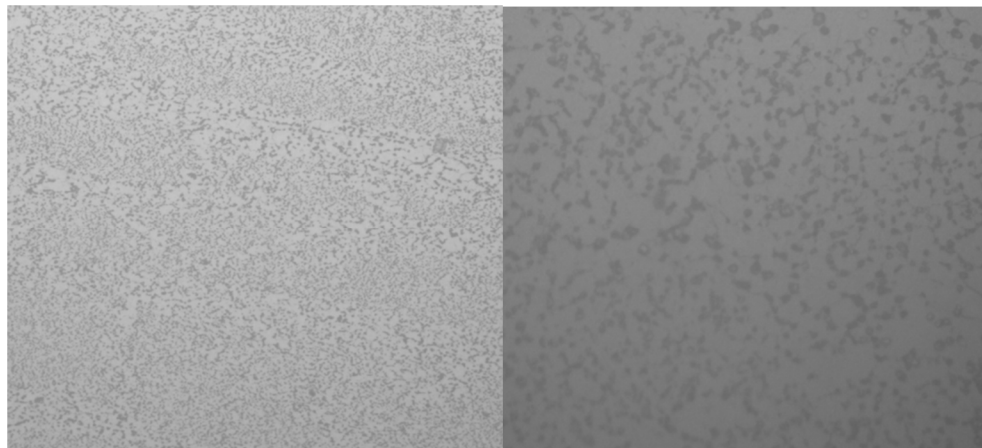
Figure 3.6. Microstructure at rim region in tangential direction at 650□ (XTL-8) with 100x & 500x magnification at the strain range 0.01235
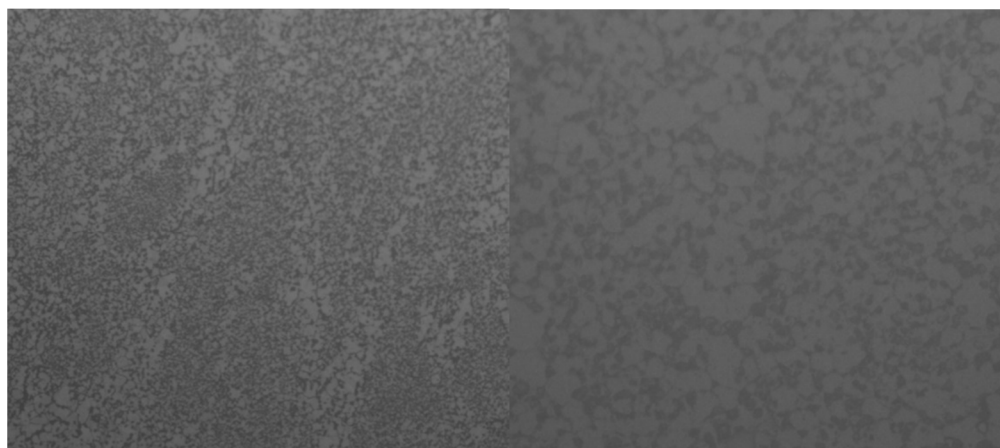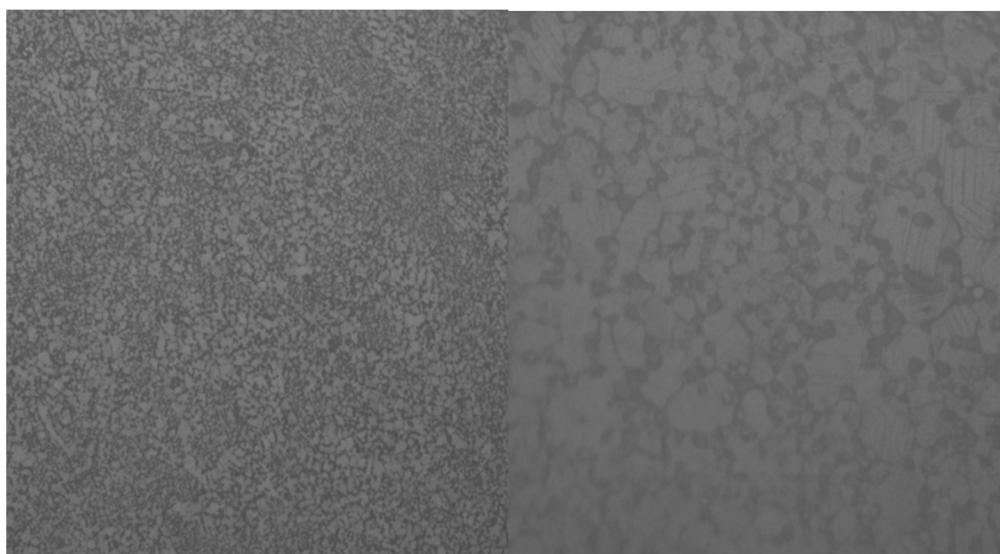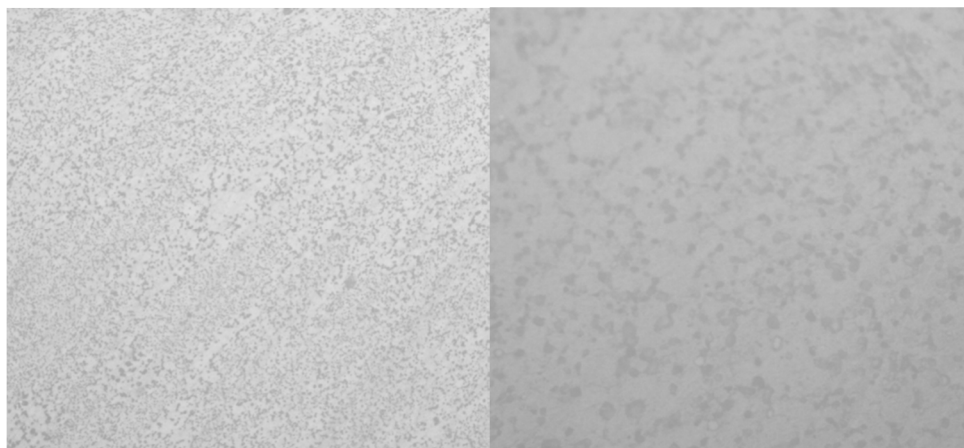

Figure 3.7. Microstructure at rim region in tangential direction at 25□ (XTL-10) with 100x & 500x magnification at the strain range 0.00665

Figure 3.8.Microstructure at rim region in tangential direction at 25□ (XTL-12) with 100x & 500x magnification at the strain range 0.01235

Figure 3.9.Microstructure at rim region in tangential direction at 750□ (XTL-14) with 100x & 500x magnification at the strain range 0.00665
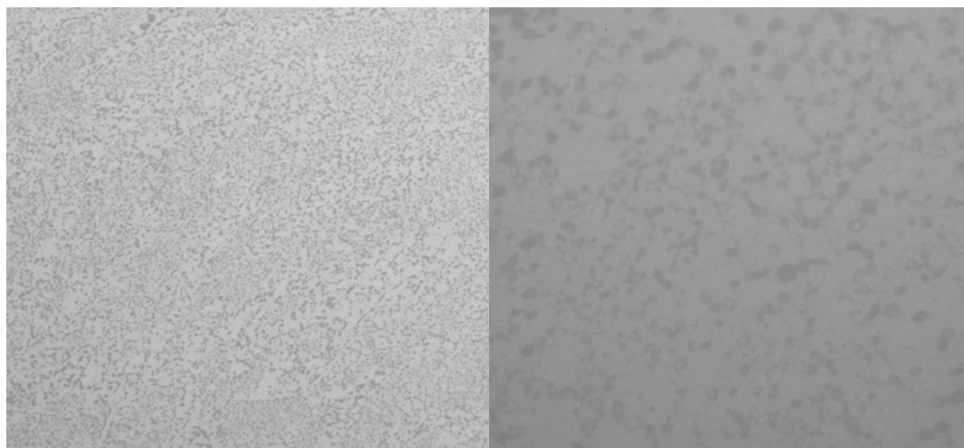

Figure 3.10.Microstructure at rim region in tangential direction at 750□ (XTL-16) with 100x & 500x magnification at the strain range 0.01235

IV.   RESULTS AND DISCUSSIONS

Life of the samples at the above-mentioned has been studied. The semi log graphical plots for variation of maximum strain against life cycles at temperatures up to 750□ are shown in the figure 4.1.
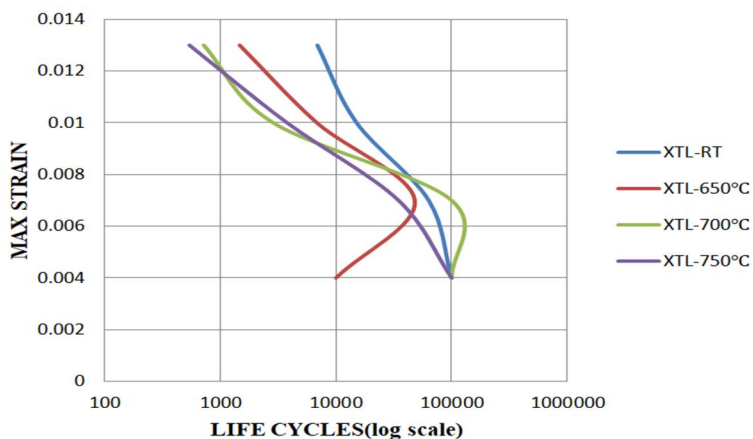

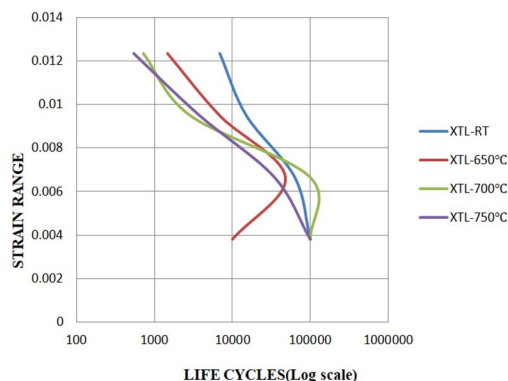Figure 4.1 Variation of maximum strain against life cycles at temperatures up to 750□

Figure 4.2 Variation of strain range against life cycles at temperatures up to 750☐

From the semi-log graphs (fig 4.1 to 4.2), the results of fatigue tests consistently showed that the fatigue life is reducing with the increase of max strain and total strain range at different temperatures ranging from room temperature to 750☐. The life of the material is less affected by the change in temperature and more affected by the strain. The reduction of fatigue life is due to the effect of the total strain range and microstructure evolution during high temperatures. Although alloy 720 has many superior properties, many researches have reported that the no. of cycles of the failure varies widely at high temperature.
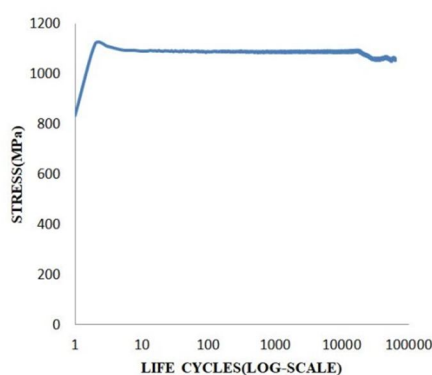

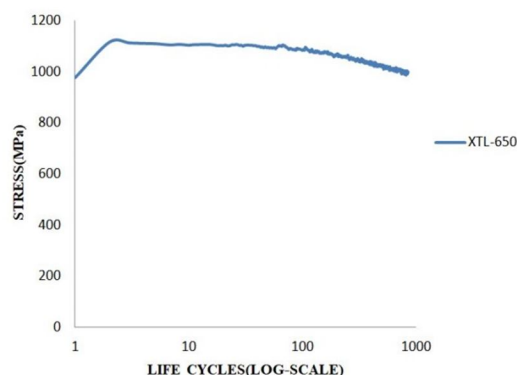Figure 4.3 S-N curve for tangential loaded specimen at rim section at room   Figure 4.4 S-N curve for tangential loaded specimen at rim section at 650℃ at Max strain at 0.013 temperature at Max strain at 0.007

In the figure 4.3, semi log S-N curve for tangential loaded specimens taken from rim region is plotted at maximum strain of 0.007. A decrease in stress is observed from 1120 MPa to 1090 MPa and the curve has stabilized at around 1090MPa. The sample has failed at around 63000 cycles. In the figure 4.4, semi log S-N curve for tangential loaded specimens taken from Rim region is plotted at maximum strain of 0.013. A gradual decrease in stress is observed from 1115 MPa to 1092 MPa. The sample have failed at around 1400 cycles.
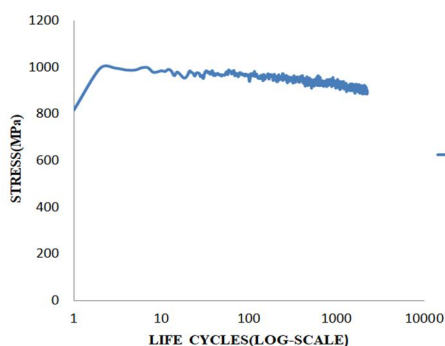

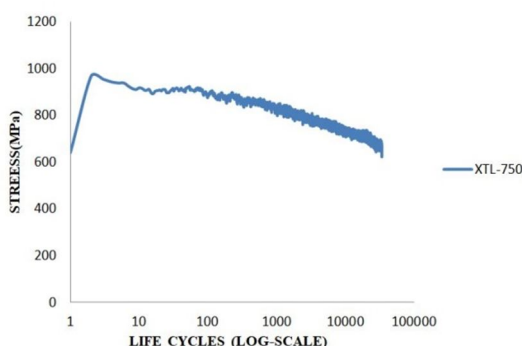Figure 4.5 S-N curve for tangential loaded specimen at rim section at 700℃ at   Figure 4.6 S-N curve for tangential loaded specimen at rim section at 750℃ at Max strain at 0.007 Max strain at 0.01

International Journal for Research in Applied Science & Engineering Technology (IJRASET)
ISSN: 2321-9653; IC Value: 45.98; SJ Impact Factor: 7.177
Volume 7 Issue VI, June 2019- Available at www.ijraset.com

In the figure 4.5, semi log S-N curve for tangential loaded specimens taken from rim region is plotted at maximum strain of 0.01. A gradual decrease in stress is observed from 1000 MPa to 890 MPa. The sample have failed at around 2800 cycles. In the figure 4.6, semi log S-N curve for tangential loaded specimens taken from rim region is plotted at maximum strain of 0.007. A slow decrease in stress is observed from 970 MPa to 680 MPa. The sample have failed at around 34000 cycles. In the figures 5.3 to 5.6, fluctuations called as serrations (zigzag pattern) are observed. This phenomenon occurs because of dynamic strain ageing (DSA). The term dynamic strain aging (DSA) refers to an aging process that takes place during plastic deformation. Over a particular range of strain rate and temperature, the interactions between solute atoms and dislocations result in a strong pinning of dislocations responsible for strain aging. Higher stress levels are required to produce further material strain, either to pull dislocations free from the pinning atoms or to nucleate fresh dislocations. Thus, the main effects of dynamic strain aging on the mechanical properties of materials during cyclic tests are an inverse dependence of the peak tensile stress on strain rate, an unusual increase in cyclic hardening and aerated flow known as the Portevin–Le Chatelier (PLC) effect. The appearance of serrations provides information that is useful to determine the kinds of atoms that interact with dislocations to cause DSA. Within a certain regime of temperature and strain rate, serrations in the flow stress–strain curves occur during plastic deformation of alloys containing interstitial or substitution solutes.

In Coffin-Manson and Ramberg-Osgood models, a low cycle fatigue cycle consists of both plastic and elastic strains. The data obtained from the machine contains the cyclic stress against strain loops at each cycle. For plotting the Coffin-Manson equation, plastic strain at half life cycle is found out from the hysteresis loop (cyclic stress – strain loop). According to Plastic flow law relationship the applied stress range $\Delta\sigma$, plastic strain range $\Delta\varepsilon_p$ and frequency ν can be defined as follows:

$$\Delta\sigma = A'\Delta\varepsilon_p^{\alpha}\nu^{\beta} \dots\dots\dots\dots\dots\dots (4.1)$$

Here A' is a numerical constant and ν is the cycling frequency. When frequency ν is constant, Eq. (4.1) can be rewritten as

$$\alpha = \left(\frac{\Delta\log\Delta\sigma}{\Delta\log\Delta\varepsilon_p}\right)_{\nu} \dots\dots\dots\dots\dots\dots (4.2)$$

The classical method works with real stresses and strains, uses a Ramberg–Osgood description for the stress-strain hysteresis loops, and considers the cyclic softening or hardening of the material, but not its transient behaviour from the monotonic stress-strain curve. The above Eq. (4.2) can be written in the below form according to Ramberg-Osgood which is analogous to Holloman Equation:

$$\text{Alternating stress } (\sigma_a) = \frac{\Delta\sigma}{2} = K' * \left(\frac{\Delta\varepsilon_p}{2}\right)^{n'} \dots\dots\dots\dots\dots\dots (4.3)$$

Where, K' is cyclic strength hardening coefficient and n' is cyclic strain hardening exponent. Values for the cyclic hardening exponent n' are typically between 0.05 and 0.3.

The Coffin-Manson plot is plotted on a log – log scale between reversals to failure $(2N_f)$ against plastic strain amplitude $(\Delta\varepsilon_p/2)$ at half- life cycle. Half-life is the half of the failure life cycle of the specimen. A reversal is 2*(No. of cycles). The Hysteresis loop for a sample at half – life cycle is shown in the figure 4.7. The width of the loop at the centre (mean stress) is taken as the plastic strain. Position and Orientation, Graphs have been plotted for samples taken from rim at tangential loading i.e., XTL. As the number of specimens extracted from these regions is more and more tests are conducted for tangential loading in Rim we have enough data for XTL to plot Coffin-Manson and Ramberg-Osgood equations. The graphs thus plotted are shown in the figures 4.8 to 4.11:
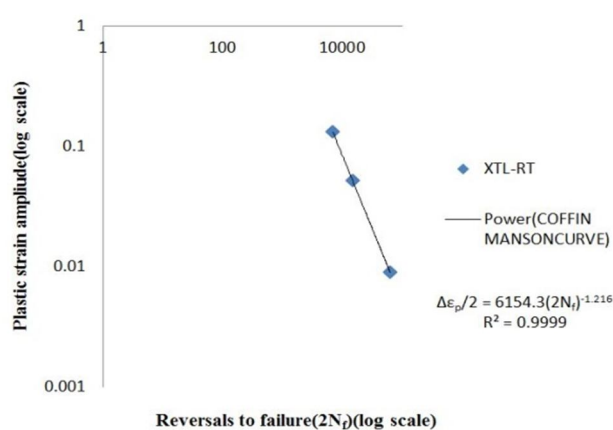

Figure 4.8. Coffin-Manson plot at rim region of disc at room temperature
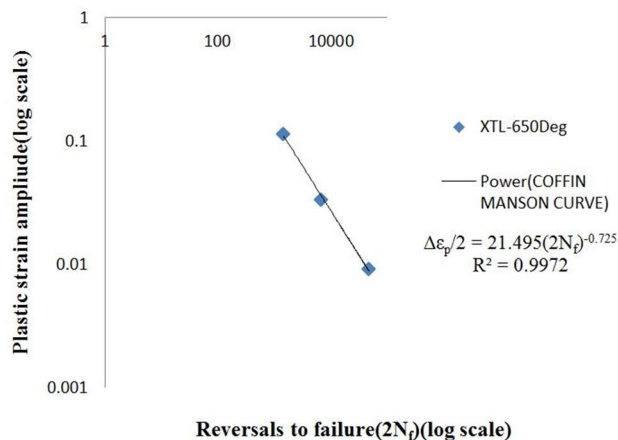
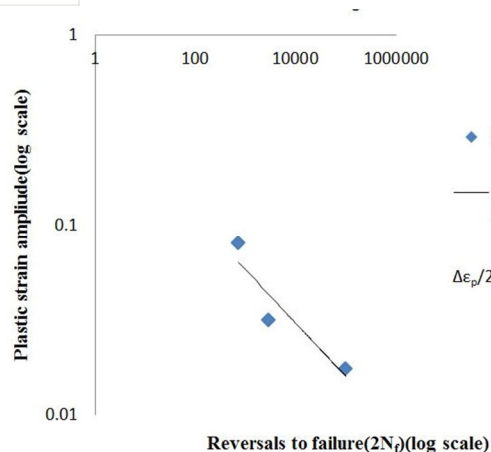Figure 4.9. Coffin-Manson plot at rim region of disc at 650℃

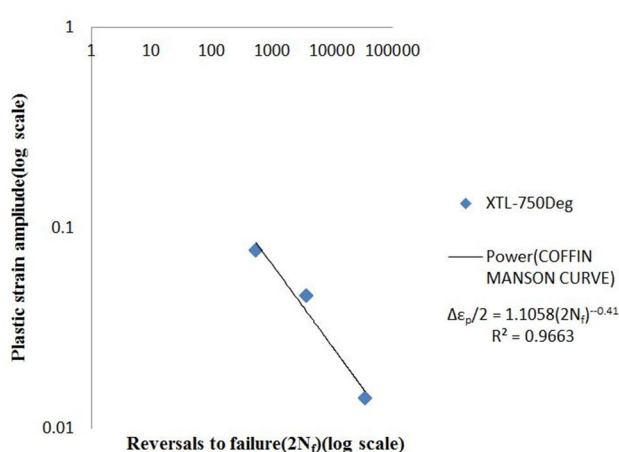Figure 4.10 Coffin-Manson plot at rim region of disc at 700℃   Figure 4.11 Coffin-Manson plot at rim region of disc at 750℃

Amongst all the coffin Manson plots, more convergence is observed for the graphs plotted at a position with respect to orientation(XTL) as shown in the figures 4.8 to 4.11. More convergence implies more idealness in the linearity of the power curve in log-log plot. More the linearity, higher is the validation of Coffin-Manson rule.

V. CONCLUSIONS

In this paper, a considerable decrease in the fatigue properties is observed with increase in the temperature and large variation in stresses is observed from room temperature (24°C) to 750°C. It can be said that the material Su-720 is recommendable to be used at high temperatures. The results of fatigue tests consistently showed that the fatigue life was reduced according to increase in the total strain ranges acquired partly from the activation of slip system and increase in plastic deformation. The cyclic stress response was decreased as total strain range increased. The decrease in peak flow stress as cyclic softening is characteristic of solute drag creep deformation. The fatigue properties are more ideal at a particular position and orientation taken together at higher convergence. All the testing has been done at a constant strain frequency (v) i.e., 0.3Hz.Butunder practical circumstances, varying frequencies have to be encountered. Hence further study of the change in Low Cycle Fatigue properties with frequency is definitely required. By studying the report, the limitations like change in fatigue resistance with temperature could be overcome by selecting the suitable alloying components which serve the purpose.

REFERENCES

[1] H. K. D. H. Bhadeshia, (1997) Re-crystallisation of Practical Mechanically Alloyed Iron–Base and Nickel–Base Superalloys, Materials Science and Engineering, A223, pp. 64-77

[2] H.W.Zhang, X.Z.Qin, X.W. Li and L.Z.Zhou, (2018). Effect of minor additions on the microstructures and stress rupture properties of a directionally solidified Ni-based superalloy, Materials Science and Engineering: A, 711, (303).

[3] J. Stringer, (1999) The role of the coating and super alloy system in enabling advanced land-based combustion turbine development. In P. J. Maziasz, I. G. Wright, W. J. Brindley, J. Stringer and C. O'Brien, eds, Gas Turbine Materials Technology (Materials Park, OH: ASM International).

[4] R. D. Kissinger, (1991) "Trends and Near Term Requirements for GE Aircraft Engines -- Titanium and Nickel Base Disk Alloys" (Paper presented at Electron Beam Melting and Refining -- State of the Art 1991, Reno, Nevada, 13-15 November)

[5] K. 0. Yu and J. A. Dominque, (1989) "Control of Solidification Structure in VAR and ESR Processed Alloy 718 Ingots" (Paper presented at the International Symposium on the Metallurgy and Applications of Super alloy 7 18, Pittsburgh, Pennsylvania, 12- 14 June) pp. 33-48.

[6] J.T.Cordy, S.L. Kelley, and L.W. Lherbier, (1984) "Chemistry and Structure Control in Re-melted Super alloy Ingots" (Paper presented at the 1984 Vacuum Metallurgy Conference on Specialty Metals Melting and Processing, Pittsburgh, Pennsylvania, 11-13 June, pp. 69- 74)

[7] A. Mitchell, (1989) "The Present Status of Melting Technology for Alloy 7 18" (Paper presented at the International Symposium on the Metallurgy and Applications of Super alloy 718, Pittsburgh, Pennsylvania, 12-14 June) pp. 1-15.

[8] J. M. Moyer, L. A. Jackman, C. B. Adasczik, R. M. Davis, and R. Forbes-Jones Teledyne Allvac (1998) Advances in Triple Melting superalloys 718,706, AND 720 P.O. Box 5030 2020 Ashcraft Avenue Monroe, North Carolina 28 11 O-5030

[9] F. E. Sczerzenie and G. E. Maurer (1982) Development of Udimet 720 for High Strength Disk Applications, Special Metals Corporation, New Hartford, NY 13413 USA

[10] Minoru Doi, Daisuke Miki, Tomokazu Moritani and Takao Kozakai (1989) Gamma/gamma-prime microstructure formed by phase separation of gamma-prime precipitates in a ni-al-ti alloy Department of Materials Science and Engineering, Nagoya Institute of Technology Gokiso-cho, Showa-ku, Nagoya 466-8555, Japan

[11] C. T. Sims, N. S. Stoloff and W. C. Hagel, (1987) eds, Super alloys II: High-Temperature Materials for Aerospace and Industrial Power (New York: John Wiley and Sons).

[12] K. A. Green, T. M. Pollock, H. Harada et al., eds., Super alloys (2004), Proceedings of the Tenth International Symposium on the Super alloys (Warrendale, PA: The Minerals, Metals and Materials Society (TMS)).

[13] S. M. Humayun Kabir, Tae-in Yeo (2001) Influence of temperature on a low-cycle fatigue behavior of a ferritic stainless steel Department of Mechanical Engineering, Chittagong University of Engineering and Technology, Chittagong-4349, Ulsan pp. 680-749

[14] Alberto Orozco-Caballero, (1972) Feng Li, Daniel Esqué-de los Ojos, Michael D. Atkinson, João Quinta da Fonseca A.M. Grade, A.T. Santhanam, R.E. Reed-Hill,Acta- On the ductility of alpha titanium: The effect of temperature and deformation mode Metal. 20 pp. 215–220.

[15] Dong-Cherng Wen , (2003) Influence of Hot Rolling and Post-Tempering on the Mechanical Properties of Duplex Stainless Steel Containing Martensite and Ferrite, Department of Mechanical Engineering, China Institute of Technology

[16] J. Cheng, S. Nemat-Nasser, (July 2000) Model for experimentally-observed high-strain-rate dynamic strain aging in titanium Article in Acta Materialia 48(12):pp.3131-3144.

[17] Sandhya, R. ; Bhanu Sankara Rao, K. ; Mannan, S. L. ; Devanathan, R. (2001) Substructural recovery in a cold worked Ti-modified austenitic stainless steel during high temperature low cycle fatigue International Journal of Fatigue, 23 (9) pp. 789-797. ISSN 0142-1123.

[18] S. Venugopal, S. Venkadesan, S.L. Mannan, J. Mater. Process. Technol. 30 (1992) Optimization of Cold and Warm Workability in 304 Stainless Steel Using Instability Maps pp.245–251.

[19] Yong Zhang, Jun Peng Liu, Shu Ying Chen, Xie Xie, Peter K. Liaw, Karin A. Dahmen, Jun Wei Qiao, Yan Li Wang Mater.Sci. Eng. A 415 (2006) Serration and noise behavior in materials pp.53

[20] X.Q. Shi a, H.L.J. Pang b , W. Zhou b , Z.P. Wang (1999) Low cycle fatigue analysis of temperature and frequency effects in eutectic solder alloy Gintic Institute of Manufacturing Technology, Nanyang Drive, Singapore 638075, Nanyang Technological University, Singapore

[21] M.A. Meggiolaro, J.T.P. Castro (2004) Statistical evaluation of strain-life fatigue crack initiation predictions Mechanical Engineering Department, Pontifical Catholic University of Rio de Janeiro (PUC-Rio), Rua Marqueˆs de Sa˜ o Vicente 225, Rio de Janeiro, RJ 22453-900, Brazil

[22] Landgraf, R.W., Morrow, J.D. and Endo, T (1987) "A cyclic constitutive relation for multi axial stress states" International Conference on Low Cycle Fatigue and Elastic-Plastic Behaviour of Materials (2nd: 1987: Munich, Germany), Elsevier applied science publishers l to ISBN-13: 978-94-010-8049-1.pg.165-170.

[23] Randy Bowman, Stephen d. Antolovich, (January 1988), Effect of melt spinning on the microstructure and mechanical properties of three Ni-base superalloys, Volume 19, Issue 1, pp 93–103

INTERNATIONAL JOURNAL
FOR RESEARCH

IN APPLIED SCIENCE & ENGINEERING TECHNOLOGY

Call : 08813907089 ◯ (24*7 Support on Whatsapp)